ACS Catalysis

Research Article

pubs.acs.org/acscatalysis

Correlating Catalytic Methanol Oxidation with the Structure and Oxidation State of Size-Selected Pt Nanoparticles

Lindsay R. Merte,[†] Mahdi Ahmadi,[†] Farzad Behafarid,[†] Luis K. Ono,[†] Estephania Lira,[†] Jeronimo Matos,[†] Long Li,[‡] Judith C. Yang,[‡] and Beatriz Roldan Cuenya*[,†]

[†]Department of Physics, University of Central Florida, Orlando, Florida 32816, United States

[‡]Department of Chemical and Petroleum Engineering, Department of Physics, University of Pittsburgh, Pittsburgh, Pennsylvania 15261, United States

Supporting Information

ABSTRACT: We have investigated the structure and chemical state of size-selected platinum nanoparticles (NPs) prepared by micelle encapsulation and supported on γ-Al_2O_3 during the oxidation of methanol under oxygen-rich reaction conditions following both oxidative and reductive pretreatments. X-ray absorption near-edge structure (XANES) and extended X-ray absorption fine-structure (EXAFS) spectroscopy measurements reveal that in both cases, the catalyst is substantially oxidized under reaction conditions at room temperature and becomes partially reduced when the reactor temperature is raised to 50 °C. Reactivity tests show that at low temperatures, the preoxidized catalyst, in which a larger degree of oxidation was observed, is more active than the prereduced catalyst. We conclude that the differences in reactivity can be linked to the formation and stabilization of distinct active oxide species during the pretreatment.

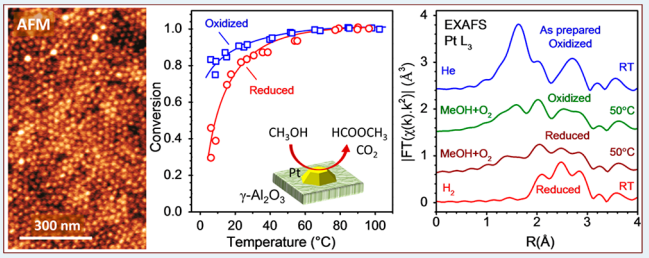

KEYWORDS: *platinum, methanol oxidation, operando, XAFS, EXAFS, XANES, alumina, nanoparticle, size-selected*

1. INTRODUCTION

The partial and total catalytic oxidation of methanol are important chemical processes, the former being employed in the synthesis of industrially relevant compounds such as formaldehyde[1,2] and methyl formate,[3,4] and the latter in the elimination of this toxic chemicals, along with other volatile organic compounds, from exhaust gases.[5−7] While partial oxidation reactions are carried out using coinage metals or various metal oxides,[8] total oxidation is typically achieved with platinum or palladium, which are able to convert methanol, higher alcohols, hydrocarbons, and carbon monoxide to CO_2 with high efficiencies at relatively low temperatures. Although occurring in a rather different environment, the electrocatalytic oxidation of methanol, which proceeds over Pt-based catalysts, is also relevant. The rate of this process is a limiting factor in the performance of direct methanol fuel cells, which produce electricity from liquid fuel without the need for reforming.[9,10]

Despite having been studied for decades, some controversy exists regarding the mechanisms of oxidation reactions over platinum, particularly regarding the formation and participation of oxide phases in the reaction process. On one hand, formation of surface oxides has long been believed to cause deactivation of Pt catalysts, for example, in the oxidation of alcohols to aldehydes and ketones.[11−13] On the other hand, chiefly in the context of CO and CH_4 oxidation, studies on single crystal samples and real catalysts have suggested that oxides may form under reaction conditions that do not hinder the oxidation reaction but, in fact, enhance the activity or modify the selectivity.[14−17] Although the topic remains a matter of debate,[18,19] operando studies of nanoparticle (NP) samples on high-surface-area supports have supported the idea that in some cases, surface oxides might enhance the activity in oxidation reactions.[20−25]

One of the primary limitations in the study of supported catalytic materials under realistic reaction conditions is the complexity of such materials and the resulting difficulty in characterizing them in detail. An emerging, successful approach to reducing the complexity of such materials, enabling more detailed characterization without sacrificing the direct applicability of the results to commercially relevant chemical processes, is to use NP synthesis techniques that produce catalysts with well-defined sizes and shapes.[26] Taking this approach, we have used reverse micelle NP synthesis to study methanol oxidation over a Pt/γ-Al_2O_3 catalyst, with particular attention to the evolution of the structure and oxidation state of Pt under reaction conditions. On the basis of the knowledge of the chemical state of the catalyst at work that can be achieved via X-ray absorption fine-structure spectroscopy (XAFS), the effect of oxidative and reductive pretreatments on the catalyst's activity and selectivity will be discussed.

Received: March 27, 2013
Revised: May 16, 2013
Published: May 17, 2013

2. EXPERIMENTAL METHODS

The Pt-loaded micellar precursor was synthesized by dissolution of H_2PtCl_6 into a solution of polystyrene-*b*-poly(2-vinylpyridine) [PS(27700)-*b*-P2VP(4300)] block copolymer (Polymer Source, Inc.) in toluene (50 mg/mL). This results in reverse micelles with the Pt salt dissolved in the P2VP core. The quantity of platinum salt added was chosen to give a Pt/P2VP molar ratio of 0.2. The mixture was stirred for 2 days to ensure complete dissolution and then filtered. The formation of uniform micelles was checked by dip-coating a natively oxidized Si wafer with the micellar solution and imaging the wafer in an atomic force microscope (AFM). The solution was then mixed with commercial γ-Al_2O_3 powder (Inframat Advanced Materials, ~150 m^2/g) to yield a nominal Pt loading of 1%. The toluene was evaporated under mechanical agitation at 50 °C. The polymer was removed by calcination in 70% O_2 (balanced with He) at 375 °C for 24 h. Complete removal of the polymer was confirmed by checking the C-1s X-ray photoelectron spectroscopy (XPS) signal, which showed only small intensity attributable to adventitious carbon accumulated during the brief exposure of the sample to air in the course of its ex situ transfer to the XPS chamber.[23,27]

AFM measurements were conducted in tapping mode with a Veeco Multimode microscope. XPS measurements were conducted using a monochromatic Al Kα X-ray source (1486.6 eV) and a Phoibos electron energy analyzer (SPECS, GmbH). Binding energies were referenced to the Al-2p photoemission peak of Al_2O_3 at 74.3 eV. Pt-4f photoemission peaks were not detectable for this sample because of their coincidence with the Al-2p peaks of the support, so the Pt-4d region was used instead to characterize the Pt oxidation state. High-angle annular dark field scanning transmission electron microscopy (HAADF-STEM) measurements were conducted after the EXAFS experiments using a JEOL JEM-2100F TEM/STEM operated at 200 kV. The TEM samples were prepared by making an ethanol suspension of the Pt/γ-Al_2O_3 powder and placing a few drops of this liquid onto an ultrathin C-coated TEM grid. The probe size of the STEM mode is about 0.2 nm. The Pt NP diameters were determined by measuring the full width at half-maximum of the HAADF intensity profile across the individual Pt NPs.

Catalytic tests were performed at the University of Central Florida (UCF) at atmospheric pressure in a vertically mounted quartz tube continuous flow reactor with either 50 mg of pure Pt/γ-Al_2O_3 catalyst or 1 mg Pt/γ-Al_2O_3 diluted with 200 mg α-Al_2O_3, in both cases supported by a quartz wool plug. The reactant mixture consisted of 4% O_2 and 0.15% methanol by volume, balanced with He. The methanol was introduced to the mixture by passing He gas through a bubbler at ambient temperature. Gas concentrations were varied using mass flow controllers (MKS), and the total flow rate was set to 50 sccm. Prior to catalytic testing, the catalyst was first reduced in H_2 (50% in He) at 240 °C for 30 min. To test the influence of the catalyst oxidation state on its catalytic activity, the reduction step was followed by an oxidation step in O_2 (70% in He) at 240 °C for 30 min. The methanol, carbon dioxide, and methyl formate concentrations were measured with an online mass spectrometer (Hiden HPR20) sampling the reactor outlet. Conversion versus temperature measurements were carried out in two different ways. For testing the reactivity of the pure catalyst, the catalyst temperature was varied manually between 5 and 100 °C by cooling the quartz reactor cell with isopropyl alcohol, passed through a coil wrapped around the reactor tube, and counter-heated with a heating tape powered by a variable-voltage AC transformer. Measurements were made in increasing temperature steps, and the conversion was allowed to reach a steady state at each temperature. For testing the reactivity of the diluted catalyst, the temperature was controlled with a tube furnace and a PID controller (Watlow) and ramped from 30 to 150 °C and then back at a rate of 10 °C/hour while monitoring the reactant and product concentrations continuously.

XAFS spectra were acquired at the Pt-L_3 edge in transmission mode at beamline X18B at the National Synchrotron Light Source (NSLS I), Brookhaven National Laboratory (BNL). Spectra were recorded from 150 eV below the absorption edge to 1230 eV above the edge (k_{max} = 18 $Å^{-1}$). The reactor used for the operando XAS measurements consisted of a Kapton tube into which 25 mg of undiluted catalyst powder was loaded and held in place by quartz wool plugs, forming a catalyst bed ~10 mm in length. The same space velocity (25 sccm total flow), gas concentrations, and pretreatment conditions were used at BNL and UCF for the reactivity measurements. During the XAFS measurements, reactants and products were monitored via an online mass spectrometer (SRS RGA100). Details of these measurements are given in Supporting Information Figure S1.

The Athena and Artemis programs[28] were used for normalization, background subtraction, and fitting of the extended X-ray absorption fine-structure (EXAFS) spectra. Theoretical scattering amplitudes and phase shifts used in the fits were calculated with the FEFF8 ab initio code[29,30] using fcc Pt to simulate Pt−Pt scattering paths and $Na_2Pt(OH)_6$ to simulate Pt−O scattering paths. To provide absolute energy calibration, the EXAFS spectrum of a Pt foil placed after the sample was measured simultaneously. Energies given in this work are referenced to the first inflection point of the Pt foil spectrum defined to be 11564 eV.

3. RESULTS

3.1. Sample Characterization. An AFM image of the Pt-loaded PS-b-P2VP micelles used as the precursor to prepare the γ-Al_2O_3-supported NP catalyst is shown in Figure 1a. The strong quasi-hexagonal ordering and uniform interparticle separation (~27 nm) observed for the dip-coated sample indicate the successful synthesis of monodisperse micelles, consistent with previous reports utilizing this method.[31−33] After impregnating the micelles onto γ-Al_2O_3 powder and removing the polymer by heating in oxygen, the XPS spectrum, showing a Pt $4d_{5/2}$ photoemission peak at 316.9 eV (Figure 1b), revealed that the sample contained oxidized platinum.[34] STEM measurements of the sample after the operando XAFS experiments revealed small Pt particles with an average diameter of 0.7 nm, distributed with a standard deviation of 0.2 nm (Figures 1c,d). According to our previous work,[27,35] no sintering is expected after our in situ treatments during the XAFS measurements which involved annealing treatments in H_2 and O_2 up to only 240 °C and in a mix of methanol and O_2 up to 50 °C.[27,35]

3.2. Catalytic Activity. Catalytic activity of the undiluted Pt/γ-Al_2O_3 sample for methanol oxidation was tested at temperatures between 5 and 100 °C following a reductive and an oxidative pretreatment, respectively, and measured conversions are plotted in Figure 2. Each experiment was performed twice using untreated catalyst samples, and the

dx.doi.org/10.1021/cs400234h | ACS Catal. 2013, 3, 1460−1468

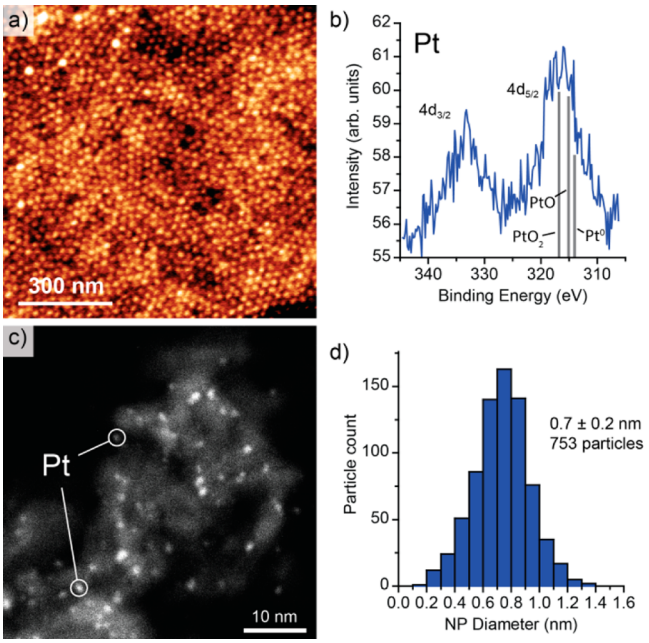

Figure 1. (a) AFM image of the Pt-loaded PS-*b*-P2VP micellar precursor used to prepare the Pt/γ-Al_2O_3 catalyst used in this study. Micelles were dip-coated onto an SiO_2/Si(111) wafer for imaging; polymer ligands were not removed. (b) Pt-4d XPS spectrum of the as-prepared (after calcination in oxygen) Pt/γ-Al_2O_3 catalyst. Binding energies expected for Pt, PtO, and PtO_2 are indicated. (c) HAADF-STEM image of the Pt/γ-Al_2O_3 catalyst after ligand removal and after operando XAFS measurements. (d) Particle size distribution extracted from HAADF-STEM measurements.

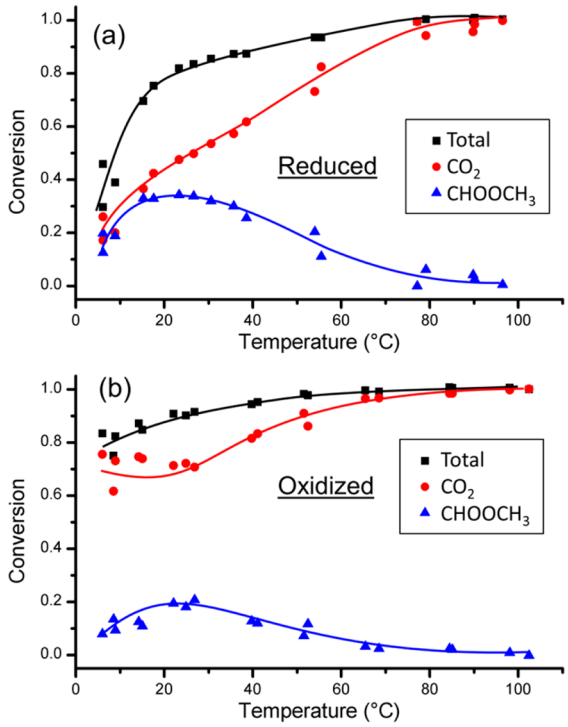

Figure 2. Reactivity of the undiluted Pt/γ-Al_2O_3 catalyst for methanol oxidation following (a) reductive (240 °C in 50% H_2 for 30 min) and (b) oxidative (240 °C in 70% O_2 for 30 min.) pretreatments. Conversion refers to the molar fraction of methanol in the feed converted to a particular product. Plotted points are individual measurements, and solid curves are guides to the eye. Carbon dioxide (CO_2) and methyl formate ($CHOOCH_3$) were the only products detected in significant quantities. All data shown correspond to steady-state reaction conditions at each given temperature.

measurements are plotted together. The only products detected were carbon dioxide (CO_2) and methyl formate ($CHOOCH_3$), as expected from the following reaction pathways:

$$2CH_3OH + 3O_2 \rightarrow 2CO_2 + 4H_2O \quad (1)$$

$$2CH_3OH + O_2 \rightarrow CHOOCH_3 + 2H_2O \quad (2)$$

At low temperatures, the total conversion over the preoxidized catalyst was significantly higher than that observed for the reduced catalyst. At 5 °C, the lowest temperature at which reactivities were tested, the oxidized catalyst converted ~80% of the methanol, wheras the reduced catalyst converted only ~40%. Product selectivities were also different for the two pretreatments, even after accounting for the differences in overall conversion. Over the prereduced catalyst at 80% conversion (observed at about 22 °C), selectivity to methyl formate was ~40%, and over the oxidized catalyst at the same total conversion (observed at 5 °C), the selectivity to methyl formate was only ~12%.

To obtain more accurate quantitative measurements of methanol oxidation reaction rates above room temperature (RT), we carried out similar reactivity measurements using a diluted sample, consisting of 1 mg Pt/γ-Al_2O_3 mixed thoroughly with 200 mg of α-Al_2O_3. In this experiment, the temperature was ramped linearly from ~30 to 150 °C and back at a rate of 10 °C/min. Total conversions as well as CO_2 and methyl formate yields for the prereduced and preoxidized catalysts during the upward sweep are shown in Figures 3a and b, respectively. Measurements were constant above 120 °C and were excluded from the plots. At low temperatures (<40 °C), the oxidized catalyst was significantly more active than the reduced catalyst: the former showed ~45% conversion at 35 °C; the latter showed negligible conversion below that temperature. At higher temperatures, the conversions of both were similar, each exceeding 90% total conversion at ~60 °C and showing increased conversion to CO_2 at the expense of methyl formate with increasing temperature. Both the preoxidized and prereduced catalysts showed high selectivity to methyl formate at low temperature and complete conversion to CO_2 above ~100 °C, although the transition point (where conversions to CO_2 and methyl formate are equal) occurs at slightly higher temperature for the reduced catalyst (67 °C) compared with the oxidized one (60 °C). Reactivity measurements obtained during the subsequent downward temperature sweep are shown in Figure 3c, with those from the oxidized catalyst overlaid on those from the reduced. Differences in reactivity in this case are almost negligible, indicating that the effect of the pretreatment is lost following the initial temperature ramp to 150 °C. The low-temperature reactivities measured during the reverse temperature ramps are intermediate between those obtained for the preoxidized and prereduced catalysts during the initial upward temperature ramp, each showing conversion of ~20% at 35 °C.

3.3. XANES and EXAFS. Operando XAFS measurements were conducted under similar conditions as the catalytic tests described above. The catalyst was first reduced in hydrogen at 240 °C and characterized at 25 °C in H_2 in the reduced state. After this, the sample was exposed to the reaction mixture (MeOH and O_2) and measured at 25 and 50 °C under steady-

dx.doi.org/10.1021/cs400234h | *ACS Catal.* 2013, 3, 1460−1468

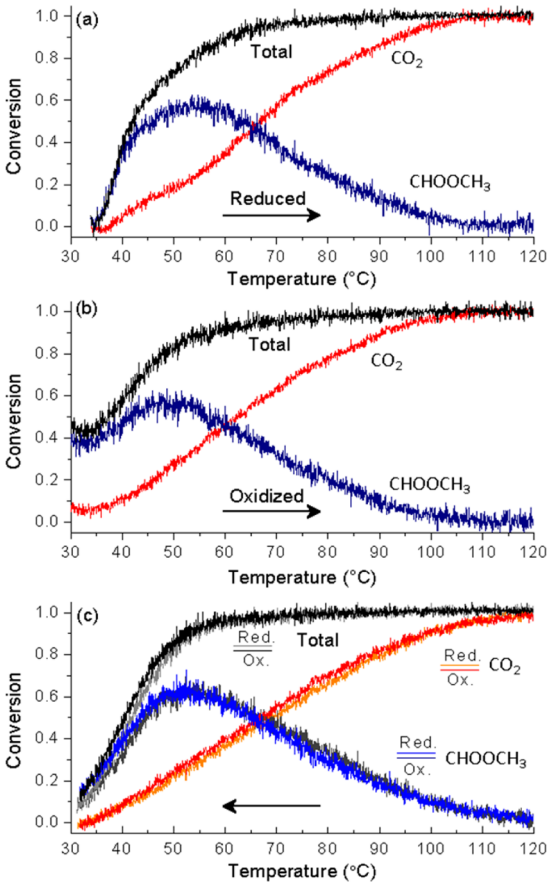

Figure 3. Reactivity of the diluted Pt/γ-Al_2O_3 catalyst for methanol oxidation. Reactivity following (a) reductive and (b) oxidative pretreatments, measured with increasing temperature. (c) Reactivity following reductive and oxidative pretreatments, measured with decreasing temperature following the measurements shown in a and b.

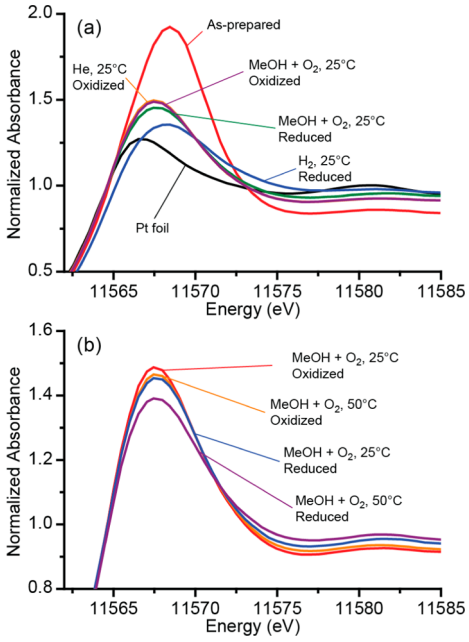

Figure 4. Pt-L_3 XANES spectra of a Pt/γ-Al_2O_3 catalyst acquired following oxidative and reductive pretreatments and under methanol oxidation conditions after these pretreatments. (a) Comparison of spectra acquired under reaction conditions at room temperature beginning in the reduced state (treated in H_2 at 240 °C) and an oxidized state (treated in O_2 at 240 °C), respectively. XANES spectra acquired of the as-prepared (oxidized) catalyst and of a bulk Pt foil are shown for reference. (b) Comparison of spectra acquired under reaction conditions at different temperatures.

state reaction conditions. After the measurements of the catalyst following the reduction pretreatment, the same sample was oxidized in O_2 at 240 °C and again exposed to the reaction mixture at 25 and at 50 °C.

Figure 4a shows XANES spectra obtained for the catalyst in the reduced state, in the oxidized state, and in the MeOH + O_2 reaction mixture, all at 25 °C, following the two different pretreatments. Similar data from a Pt foil are also included for reference. Pt-L_3 absorption spectra exhibit a prominent peak, referred to as a "white line" (WL), just above the edge, resulting from electronic transitions from $2p_{3/2}$ to 5d states. The intensity of the WL is determined primarily by the unoccupied 5d density of states and, thus, reflects the average oxidation state of the platinum atoms. The as-prepared sample, measured following a 24-h calcination in O_2 at 375 °C, exhibits an intense WL, most likely indicating that a substantial fraction of the platinum in the catalyst is in the form of PtO_2.[36−38] Compared with a metallic platinum foil, the WL of the reduced nanosized catalyst exhibits a shift to higher energy as well as some broadening due to a combination of NP size/shape effects and changes in the electronic structure resulting from hydrogen chemisorption.[39,40] Exposure of the reduced catalyst to the oxygen-rich reaction mixture led to an increase in the white line intensity and decrease in the peak energy, indicating the presence of chemisorbed oxygen on Pt or PtOx species.[38] In the case of the preoxidized sample, exposure to the reaction mixture at 25 °C led to a very slight decrease in WL intensity, indicating only a very small change in the oxygen content of the Pt NPs. However, the intensity of the WL of the prereduced sample upon exposure to the reaction mixture at 25 °C was slightly lower than that of the sample following oxidation at 240 °C.

Although the XANES spectra of the preoxidized and prereduced catalysts under reaction conditions at 25 °C are rather similar, the difference between them increased upon heating to 50 °C, as shown in Figure 4b. In both cases, heating to 50 °C led to a decrease in the WL intensity with no change in peak position, but the difference in intensity between the 25 and 50 °C data was significantly larger for the prereduced catalyst than for the preoxidized catalyst.

The EXAFS oscillations extracted from the postedge region of the Pt-L_3 absorption coefficient result from interference effects due to the scattering of emitted photoelectrons by the surrounding atoms and thus reflect the averaged local coordination environment of the Pt atoms. Fourier-transformed EXAFS spectra in Figure 5 exhibit characteristic peaks at positions corresponding roughly (neglecting element- and momentum-dependent phase shifts) to the nearest-neighbor distances in the sample. The EXAFS spectra of the Pt catalyst in the as-prepared, prereduced, and preoxidized initial states (prereaction) as well as in the MeOH + O_2 mix at 25 °C and at 50 °C are shown in Figure 5, together with the spectrum of a bulk Pt foil. The spectrum of the prereduced catalyst shows primarily a peak at ~2.6 Å (phase uncorrected) corresponding to Pt−Pt nearest-neighbor scattering, similar to that of the Pt foil, but reduced in intensity because of the small size (and thus reduced average coordination numbers) and enhanced static

dx.doi.org/10.1021/cs400234h | ACS Catal. 2013, 3, 1460−1468

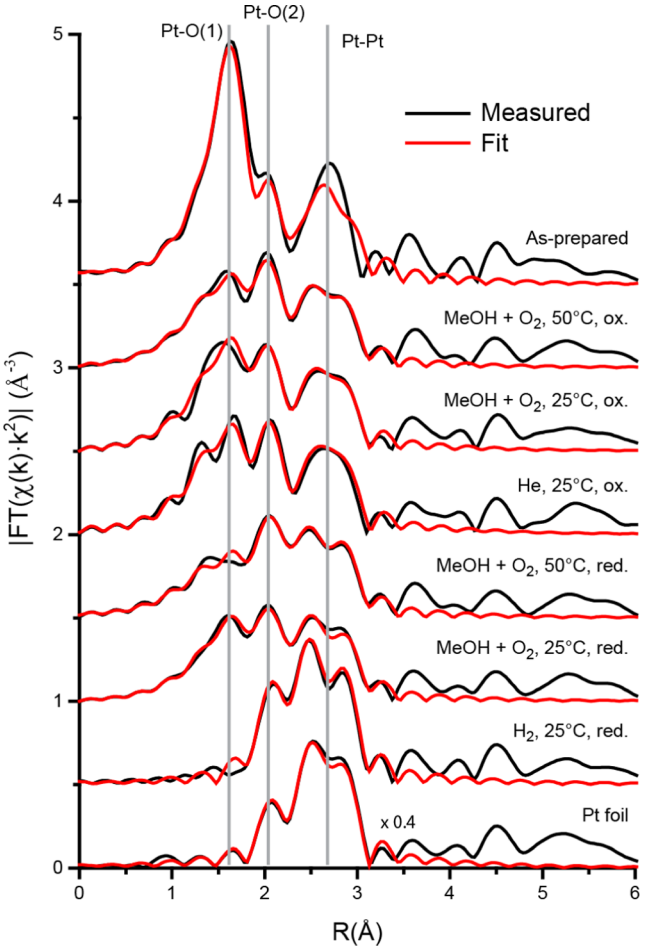

Figure 5. Fourier-transformed k^2-weighted EXAFS spectra of the Pt/γ-Al_2O_3 catalyst after reductionand oxidation and under MeOH oxidation reaction conditions following the two pretreatments leading to the oxidation and reduction of the catalysts. Shown also are first-shell fits to the experimental data using a combination of three scattering components, as described in the text. A Hanning window from 2.5 to 13 $Å^{-1}$ with Δk = 1 $Å^{-1}$ was used to compute the Fourier transforms. The data are vertically displaced for clarity.

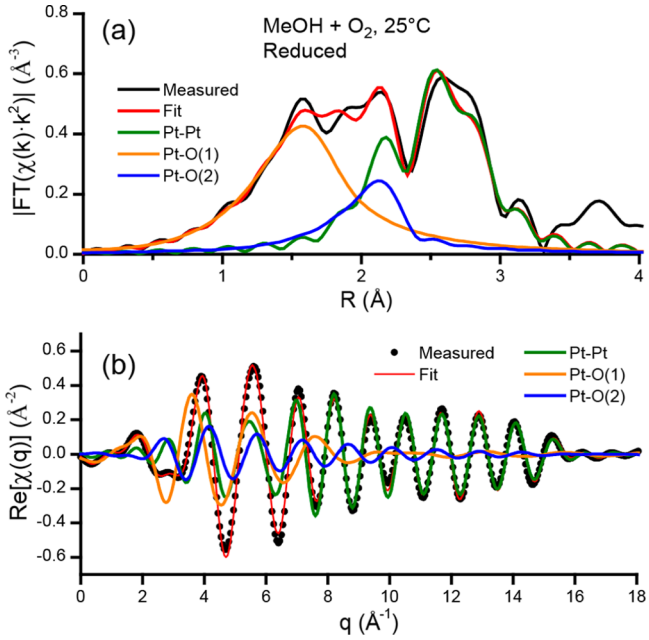

Figure 6. (a) Fourier-transformed (k = 2.5–15.5 $Å^{-1}$) EXAFS spectrum of the initially reduced catalyst measured at 25 °C in MeOH + O_2. The fitted spectrum as well as the magnitudes of the three contributing scattering components corresponding to metallic Pt, a Pt–O(1) bond at ~2.0 Å, and Pt–O(2) at ~2.5 Å are also shown. (b) Inverse-Fourier-transformed (R = 1.2–3.2 Å) EXAFS spectrum corresponding to that in part a.

atomic disorder of the NPs. The as-prepared sample (with the highest PtOx content due to its extensive oxidation at 375 °C for 24 h), in contrast, shows a dominant peak at ~1.7 Å (phase-uncorrected) due to Pt–O nearest-neighbor scattering. The spectrum of the preoxidized catalyst (O_2 treatment at 240 °C for 30 min) and those of the catalyst obtained under reaction conditions exhibit features corresponding to both Pt–Pt and oxidic Pt–O scattering [designated as Pt–O(1) in Figure 5] as well as a third feature at an intermediate scattering distance (~2.1 Å phase uncorrected) designated as Pt–O(2).

To separate and quantify the overlapping components of the EXAFS spectra, least-squares fitting was carried out using theoretically calculated scattering amplitudes and phase shifts generated using FEFF. The best fits obtained in this way are plotted together with the experimental data in Figure 5. The combination of a Pt–Pt scattering component and two Pt–O scattering components was found to adequately reproduce the experimental spectra, as suggested by the observations above. An example of one of the fits, corresponding to the initially reduced catalyst under methanol oxidation reaction conditions at 25 °C, is shown in Figure 6, with the contributions of the individual scattering components plotted separately in both r-space (Fourier-transformed) and k-space. From these fits, the following distances (phase-corrected) were obtained: Pt–Pt (2.76 Å), Pt–O(1) (2.0 Å), and Pt–O(2) (2.5 Å). The remaining fits and relevant fit information are included in Supporting Information Figures S2–S9 and Table S1.

Best fit parameters from the analysis of the EXAFS data are given in Table 1, and the Pt–Pt, Pt–O(1) and Pt–O(2) coordination numbers (CNs) are plotted in Figure 7. The fitted Pt–Pt CN for the reduced catalyst of ~7 corresponds to particles of ~1 nm in diameter,[41,42] which agrees well with the mean particle diameter d measured by STEM, provided that the volume-averaging nature of the XAFS measurement is accounted for by weighting the histogram by d^3. Although the particles measured by STEM had a mean diameter of 0.7 nm, the greater contribution of larger particles results in an apparent diameter (volume-weighted) of 0.9 nm. The Pt–O(1) scattering component of the EXAFS spectra, with a bond length of 2.0 Å, is typical of strong platinum–oxygen bonds, and its appearance upon exposure of the reduced catalyst to the reaction mixture and after oxidation treatments, concomitant with a decrease in the Pt–Pt coordination number, indicates that we do not have chemisorbed oxygen on Pt, but the formation of platinum oxides.

Consistent with the XANES measurements, more extensive oxidation is observed following the oxygen pretreatment at 240 °C than during exposure of the reduced catalyst to methanol and oxygen at 25 °C, and little change in the oxidation state is observed after exposure of the oxidized catalyst to the reactant mixture. Determination of the extent of oxidation and of the stoichiometric ratio of the oxides formed is not straightforward. Since both the XANES and EXAFS spectra give averaged information for the entire sample, it is difficult to distinguish between a mixture of phases and a single phase of intermediate

dx.doi.org/10.1021/cs400234h | ACS Catal. 2013, 3, 1460–1468

Table 1. Pt L_3 EXAFS Fit Parameters for the Pt/γ-Al_2O_3 Catalyst in the As-Prepared, Reduced and Oxidized States As Well As under Methanol Combustion Conditions Following Reducing and Oxidizing Pretreatments[a]

	n_{Pt-Pt}	d_{Pt-Pt} (Å)	$n_{Pt-O(1)}$	$d_{Pt-O(1)}$ (Å)	$n_{Pt-O(2)}$	$d_{Pt-O(2)}$ (Å)
as-prepared	4.1 ± 0.3	2.763 ± 0.010	3.7 ± 0.6	1.98 ± 0.02	1.7 ± 0.6	2.51 ± 0.05
reduced H_2, 25 °C	7.3 ± 0.7	2.760 ± 0.004			0.5 ± 0.3	2.51 ± 0.02
reduced MeOH + O_2 25°C	4.6 ± 1.0	2.760 ± 0.006	2.1 ± 0.7	2.00 ± 0.02	1.2 ± 0.8	2.52 ± 0.03
reduced MeOH + O_2 50°C	5.5 ± 1.0	2.752 ± 0.005	2.1 ± 0.7	1.97 ± 0.02	0.6 ± 0.4	2.54 ± 0.03
oxidized He, 25°C	3.1 ± 1.7	2.760 ± 0.010	2.9 ± 0.8	1.98 ± 0.03	1.0 ± 0.9	2.55 ± 0.04
oxidized MeOH + O_2 25°C	3.7 ± 0.6	2.761 ± 0.006	2.9 ± 0.6	1.99 ± 0.01	1.2 ± 0.5	2.52 ± 0.02
oxidized MeOH + O_2 50°C	4.7 ± 0.9	2.759 ± 0.006	3.2 ± 1.1	1.98 ± 0.02	1.1 ± 0.6	2.51 ± 0.02
Pt Foil	12.0 ± 0.4	2.765 ± 0.001				

[a]Fit parameters for a Pt foil are shown for reference. n_{Pt-Pt}, $n_{Pt-O(1)}$, and $n_{Pt-O(2)}$ are coordination numbers, and d_{Pt-Pt}, $d_{Pt-O(1)}$, and $d_{Pt-O(2)}$ are bond lengths for the three distinct scattering species.

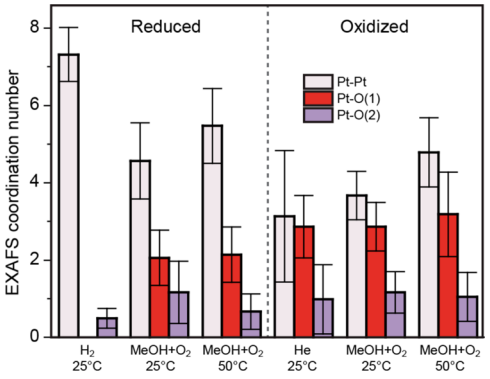

Figure 7. Coordination numbers of three different Pt species extracted from first-shell analysis of EXAFS spectra. The sample was exposed to two different pretreatments under reductive (left) and oxidative (right) conditions. Spectra were acquired under the conditions indicated, in order from left to right.

stoichiometry. The persistent presence of a metallic Pt−Pt EXAFS component following oxidative treatments appears to indicate only partial oxidation of the NPs, yielding a structure with an oxide shell around a metallic core. Nevertheless, we cannot rule out potential contributions from large grains of Pt in the sample that could be only partially oxidized, whereas the smaller NPs might be completely oxidized. Although not detected in STEM measurements of this sample, even an extremely small number of grains of only modest diameter (10−20 nm) can potentially make a detectable contribution to the XAFS spectra owing to their much greater volume.[24] We note, however, that due to the very low surface-to-volume ratio of such large grains, their contribution to the catalytic activity should in any case be negligible.

The Pt−O(2) scattering component, modeled as a platinum−oxygen bond with a length of ∼2.5 Å, could not be quantified with great accuracy because of its strong overlap with the Pt−Pt and Pt−O(1) components, but exclusion of this component led to significantly poorer fits to the EXAFS spectra. The need to include a long Pt−O component in EXAFS spectra of noble metals on various supports has been noted in several previous studies.[43−46] Koningsberger and Gates observed such a component in spectra of various catalysts, and assigned it to bonds between platinum atoms and oxide ions of the Al_2O_3 support, with the unusual length attributed to the presence of hydrogen at the interface.[12,43] A theoretical study investigating hydrogenated platinum clusters on γ-Al_2O_3 appears to support this, showing also drastic NP shape changes and breakage of Pt-substrate bonds upon adsorption of high coverages of hydrogen at the NP/support interface.[47] However, we consistently observe this long-bond component more prominently under oxidizing conditions than in the exclusive presence of hydrogen. We interpret its consistent presence under oxidizing conditions as a sign of significant contact area between the NPs and the Al_2O_3 support surface, possibly due to a modification of the NP shape (flattening) under reaction conditions. The latter is in agreement with data from Markusse et al.[12] on C-supported NPs, which suggested spherical to hemispherical (or flattened) shape transformations when reducing environments were replaced by oxidizing reaction conditions.

In agreement with the XANES measurements, which showed a decrease in WL intensity upon raising the reactor temperature to 50 °C, we observe an increase in the Pt−Pt coordination number in EXAFS spectra of both the initially reduced and initially oxidized catalysts, as would be expected upon either partial reduction of Pt oxides to Pt metal or upon changing the NP shape from a 2D to 3D morphology. Such a transformation would also be expected to lead to a decrease in Pt−O(1) and Pt−O(2) coordination numbers, which is not clearly observed, although the latter changes may be within the uncertainty of the measurements.

4. DISCUSSION

Our experiments reveal that Pt NP/γ-Al_2O_3 catalysts exhibit a complex behavior in the oxidation of methanol that is substantially different from that of bulk Pt. Over pure Pt wire catalysts, McCabe and McCready[48] found that methanol oxidation exhibited reaction kinetics similar to CO oxidation, which is characterized by CO-saturated surfaces and low activity at low temperatures, versus oxygen-saturated surfaces and high activity at high temperature. It was therefore proposed that methanol oxidation over Pt proceeds through a strongly bound intermediate, such as CO, which prevents adsorption of O_2 and thus limits the rate at low temperature. This is similar to what has been observed for electrochemical methanol oxidation over Pt/C catalysts, where poisoning of the Pt anode surfaces with CO has been directly observed and found to cause large overpotentials in the reaction.[9] However, such poisoning does not seem to occur in our experiments, since according to Safonova et al.,[49] a significant shift and broadening to higher energy of the Pt-L_3 white line is expected upon adsorption of CO, which was not observed in our data. In our experiments, XANES measurements indicate that under reaction conditions at 25 °C, the platinum catalyst is in an oxygen-rich state qualitatively similar to that of the preoxidized sample, regardless of the pretreatment.

dx.doi.org/10.1021/cs400234h | ACS Catal. 2013, 3, 1460−1468

In addition, the observation of methyl formate as the main partial oxidation product is consistent with a different mechanism for MeOH oxidation over highly dispersed Pt NPs/Al_2O_3, as compared with pure Pt.[50,51] In particular, over pure Pt catalysts, the main partial oxidation product was formaldehyde and was formed in only small yields.[48,52] For Pd/Al_2O_3 catalysts, methyl formate has been observed to be the only product formed over PdO surfaces.[53] Methyl formate production could occur through different reaction paths involving surface formate species (HCHO).[53] Our high selectivity toward CO_2 at moderate temperatures suggests that the oxidation of formate species is faster than the condensations of absorbed methoxide with HCHO, dimerization of HCHO, or esterification of formic acid (HCOOH) intermediates.[53]

Furthermore, the oxidation state effect seems to be complex, and system-dependent. For example, in methanol oxidation reactions over high surface area palladium catalysts (Pd/Al_2O_3), the reverse trend to what we observed was reported, with a higher catalytic activity[53,54] (up to 40 times) and a lower selectivity toward methyl formate[53] being detected for the reduced Pd catalysts as compared with PdO. Moreover, the methanol oxidation turnover frequency was shown to be significantly lower for smaller Pd NPs[53] because of stronger binding of chemisorbed oxygen, resulting in higher O coverages and the blockage of active sites.[55] A similar size-dependent binding was also reported for the O−Pt system,[56−58] but no poisoning due to chemisorbed oxygen was observed in our study, since both the initially reduced and initially oxidized samples were found to become/remain oxidized in the presence of the reactants (evident from the decrease in Pt−Pt coordination number and increase in Pt−O), and the sample with the highest content of oxygen (preoxidized) was also found to be the most active.

Nevertheless, although XANES and EXAFS measurements indicate that in both cases the samples are oxidized under reaction conditions, our experiments show clearly that the initial oxidation state of the Pt NPs has a strong effect on the catalysts' low-temperature reactivity and that a greater degree of oxidation leads to larger reaction rates. The results of the EXAFS analysis displayed in Figure 7 reveal a higher degree of oxidation (larger contribution of the Pt−O(1) bond) for the preoxidized NPs under reactant exposure at 25 and 50 °C. The latter finding is in accord with previous results by Markusse et al.,[12] revealing more extensive catalyst oxidation under aqueous alcohol oxidation reaction conditions after an oxidative catalyst start-up versus a reductive start-up.

It should be mentioned that in our case, the preoxidized catalyst cannot be considered a true oxygen reservoir, since the amount of oxygen stored in the form of Pt oxide is insignificant as compared with the oxygen consumed during the reaction. Therefore, if any constituents of the catalysts' lattice (in this case oxygen) leave the NP surface as part of the reaction products, they should be subsequently replenished by the oxygen reactant in the gas stream following a Mars−van-Krevelen (M−v-K) process.[59] On the other hand, a Langmuir−Hinshelwood (L−H) mechanism in which both of the reactants adsorb on the NP surface and then react has also been observed, mainly on reduced metal surfaces,[60,61] but also on some metal oxide surfaces (e.g., RuO_2).[62,63] Furthermore, in numerous previous studies, the drastic differences in reactivity observed for oxidized versus reduced catalyst have been attributed to the onset of one of the former distinct reaction mechanisms. For instance, in CO oxidation reactions over Pd catalysts, it has been shown that the Langmuir−Hinshelwood mechanism takes place over reduced Pd surfaces, but with a lower activity as compared with oxidized surfaces following Mars−van-Krevelen processes.[60,64] Similar behavior has also been reported for Pt, showing higher activity for the oxidized catalyst during CO oxidation.[14,15,65] Nevertheless, the NP/support interface and oxygen or hydroxyl exchange between the metal NP phase and the oxide support might also need to be considered.[66,67]

In our case, the difference in reactivity between the preoxidized and prereduced catalysts cannot be attributed to a distinct reaction mechanism taking place over reduced versus oxidized Pt surfaces (e.g., M−v-K vs L−H), since our operando spectroscopic characterization (XANES and EXAFS) revealed that both catalysts are oxidized under reaction conditions. In contrast, our operando data indicate that the catalytic activity of the NPs is influenced not only by the presence of oxide overlayers but also by their precise structure, chemical composition, and possibly also thickness, which likely differ due to the difference in temperature during the initial oxygen exposure (240 °C in the case of the preoxidized catalyst, 25 °C in the case of the prereduced catalyst). This is in line with previous studies showing that the catalytic activities of different PtO_x phases vary substantially. For example, theoretical calculations by Seriani et al.[68] showed that although PtO and PtO_2 layers on Pt surfaces are inert toward CO and CH_4 oxidation, a Pt_3O_4 surface can be highly active for these reactions. Other studies have shown that Pt oxides with higher oxidation states such as PtO_2 or $Pt(OH)_3$ could act as poisonous species for primary alcohol oxidation (e.g., methanol), and lower oxidation states such as PtO and Pt(OH) were identified as active species.[69] Unfortunately, EXAFS cannot be used to distinguish the different PtOx phases, since they are all characterized by a nearly identical Pt−O distance of ∼2 Å.

The differences in the XANES peak intensity and position observed between the as-prepared NPs (PtO_2-rich) and those measured under reaction conditions (Figure 4a) can serve as guidance to distinguish different chemical states of Pt in PtOx compounds. In particular, the XANES spectra of our catalyst under reaction conditions and after the oxidative pretreatment exhibit white lines which are significantly less intense than that of the as-prepared sample, measured following a 24-h calcination at 375 °C. The drastic difference in intensity, despite substantial Pt oxide formation under reaction conditions at 25 °C and in oxygen at 240 °C, is an indication that the oxides formed under these conditions consist primarily of Pt in a 2+ oxidation state, whereas the prolonged higher-temperature treatment (375 °C) likely produces Pt in the 4+ oxidation state. Such self-limiting oxidation of Pt NPs at low temperatures (and also at low potentials under electrochemical conditions[38]) has been observed in a number of studies to date. Considering that the thermodynamically favored, well-ordered PtO_2 phase has been found to be catalytically inert for a number of reactions, the existence of partially oxidized species (e.g., PtO) appears to be an important element in the high oxidation activities observed for certain catalytic reactions.[20]

Furthermore, XANES data acquired at 50 °C on the prereduced sample (Figure 4b) revealed a significant decrease in the WL intensity, not observed on the preoxidized sample, which might be assigned either to a more facile reduction of PtOx species or to the loss of chemisorbed oxygen species.

dx.doi.org/10.1021/cs400234h | ACS Catal. 2013, 3, 1460−1468

Since no significant changes are observed in the Pt−Pt and Pt−O(1) EXAFS components upon heating the sample to 50 °C, a removal of chemisorbed species (which should have a weaker overall effect on the EXAFS coordination numbers) appears more likely. Nevertheless, it should be noted that the measured catalytic activity of such sample is still lower than that of the preoxidized counterpart.

Recent theoretical and experimental studies of methanol oxidation over Pd catalysts assigned the most active Pd species to either metallic Pd or a thick and well-ordered PdO structure, with catalysts containing only one layer of oxide having higher reaction barriers and lower reactivity.[70] According to our operando spectroscopic data, it is plausible that a better-ordered oxide layer (likely PtO) might be present in the preoxidized sample, and a thinner surface oxide layer might exist under reactant exposure on the reduced sample. This might be responsible for the initially higher activity observed for our oxidized sample as compared with the reduced sample.

In summary, our study highlights the importance of the specific chemical structure (Pt coordination environment and degree of disorder) and thickness of the oxidic species formed on NPs after different sample pretreatments as well as directly under operando reaction conditions for oxidative catalytic reactions.

CONCLUSIONS

We have investigated the chemical state of micelle-synthesized Pt NPs supported on γ-Al_2O_3 under methanol oxidation reaction conditions. Reactivity measurements following oxidative and reductive pretreatments show clear differences at low temperature, with an enhanced reactivity of the oxygen pretreated NPs. The most highly active NPs are shown by XANES and EXAFS measurements to consist predominantly of platinum oxides. Similar measurements of the prereduced catalyst show that metallic NPs are also partially oxidized upon exposure to the reactants at room temperature, but with a different structure from those formed in the oxidative pretreatment at 240 °C, which makes them less active and less stable. Our study supports the notion that platinum oxides enhance the activity of oxidation catalysts at low temperature but reveals some subtleties regarding the precise nature of the oxides formed that are key for the understanding of the reactivity trends observed. In particular, our work illustrates the importance of operando studies to gain fundamental insight into structure, chemical state, and reactivity correlations of nanoscale catalysts.

ASSOCIATED CONTENT

Supporting Information

Additional information as noted in text. This material is available free of charge via the Internet at http://pubs.acs.org.

AUTHOR INFORMATION

Corresponding Author

*E-mail: roldan@ucf.edu.

Notes

The authors declare no competing financial interest.

ACKNOWLEDGMENTS

The authors acknowledge Anatoly I. Frenkel (Yeshiva University) for assistance with the evaluation of the XAFS data and Nebojsa Marinkovic (BNL) for his excellent beamline support. This work has been made possible thanks to the financial support of the Office of Basic Energy Sciences of the U.S. Department of Energy under Grants DE-FG02-08ER15995 (B.R.C.) and DE-FG02-03ER15476 (J.C.Y.). Support to beamline X18B at NSLS-BNL, where the XAFS experiments were conducted, was provided by the DOE's Synchrotron Catalysis Consortium (DE-FG02-05ER15688) and DOE-BES (DE-AC02-98CH10866). NFCF at University of Pittsburgh is acknowledged for the use of JEOL JEM-2100F.

REFERENCES

(1) Lefferts, L.; van Ommen, J. G.; Ross, J. R. H. *Appl. Catal.* **1986**, *23*, 385.
(2) Nagy, A.; Mestl, G. *Appl. Catal., A* **1999**, *188*, 337.
(3) Guerreiro, E. D.; Gorriz, O. F.; Larsen, G.; Arrúa, L. A. *Appl. Catal., A* **2000**, *204*, 33.
(4) Wittstock, A.; Zielasek, V.; Biener, J.; Friend, C. M.; Bäumer, M. *Science* **2010**, *327*, 319.
(5) Spivey, J. J. *Ind. Eng. Chem. Res.* **1987**, *26*, 2165.
(6) Sharma, R. K.; Zhou, B.; Tong, S.; Chuane, K. T.; Tg, A. *Ind. Eng. Chem. Res.* **1995**, *34*, 4310.
(7) Gandhi, H. S.; Graham, G. W.; McCabe, R. W. *J. Catal.* **2003**, *216*, 433.
(8) Tatibouët, J. M. *Appl. Catal., A* **1997**, *148*, 213.
(9) Iwasita, T. *Electrochim. Acta* **2002**, *47*, 3663.
(10) Lamy, C.; Lima, A.; LeRhun, V.; Delime, F.; Coutanceau, C.; Léger, J.-M. *J. Power Sources* **2002**, *105*, 283.
(11) Mallat, T.; Baiker, A. *Chem. Rev.* **2004**, *104*, 3037.
(12) Markusse, A. P.; Kuster, B. F. M.; Koningsberger, D.; Marin, G. B. *Catal. Lett.* **1998**, *55*, 141.
(13) Nicoletti, J. W.; Whitesides, G. M. *J. Phys. Chem.* **1989**, *93*, 759.
(14) Ackermann, M. D.; Pedersen, T. M.; Hendriksen, B. L. M.; Robach, O.; Bobaru, S. C.; Popa, I.; Quiros, C.; Kim, H.; Hammer, B.; Ferrer, S.; Frenken, J. W. M. *Phys. Rev. Lett.* **2005**, *95*, 255505.
(15) Hendriksen, B. L. M.; Frenken, J. W. M. *Phys. Rev. Lett.* **2002**, *89*, 2.
(16) Li, W.-X. *J. Phys.: Condens. Matter* **2008**, *20*, 184022.
(17) Mallens, E. P. J.; Hoebink, J. H. B. J.; Marin, G. B. *Catal. Lett.* **1995**, *33*, 291.
(18) Gao, F.; Wang, Y.; Cai, Y.; Goodman, D. W. *J. Phys. Chem. C* **2009**, *113*, 174.
(19) McClure, S. M.; Goodman, D. W. *Chem. Phys. Lett.* **2009**, *469*, 1.
(20) Alayon, E. M. C.; Singh, J.; Nachtegaal, M.; Harfouche, M.; van Bokhoven, J. A. *J. Catal.* **2009**, *263*, 228.
(21) Singh, J.; van Bokhoven, J. A. *Catal. Today* **2010**, *155*, 199.
(22) Croy, J. R.; Mostafa, S.; Heinrich, H.; Roldan Cuenya, B. *Catal. Lett.* **2009**, *131*, 21.
(23) Mostafa, S.; Behafarid, F.; Croy, J. R.; Ono, L. K.; Li, L.; Yang, J. C.; Frenkel, A. I.; Roldan Cuenya, B. *J. Am. Chem. Soc.* **2010**, *132*, 15714.
(24) Paredis, K.; Ono, L. K.; Mostafa, S.; Li, L.; Zhang, Z.; Yang, J. C.; Barrio, L.; Frenkel, A. I.; Roldan Cuenya, B. *J. Am. Chem. Soc.* **2011**, *133*, 6728.
(25) Singh, J.; Nachtegaal, M.; Alayon, E. M. C.; Stotzel, J.; van Bokhoven, J. A. *ChemCatChem* **2010**, *2*, 653.
(26) Roldan Cuenya, B. *Thin Solid Films* **2010**, *518*, 3127.
(27) Matos, J.; Ono, L. K.; Behafarid, F.; Croy, J. R.; Mostafa, S.; DeLaRiva, A. T.; Datye, A. K.; Frenkel, A. I.; Roldan Cuenya, B. *Phys. Chem. Chem. Phys.* **2012**, *14*, 11457.
(28) Ravel, B.; Newville, M. *J. Synchrotron Radiat.* **2005**, *12*, 537.
(29) Rehr, J. J.; Albers, R. C. *Rev. Mod. Phys.* **2000**, *72*, 621.
(30) Ankudinov, A. L.; Bouldin, C. E.; Rehr, J. J.; Sims, J.; Hung, H. *Phys. Rev. B* **2002**, *65*, 104107.
(31) Croy, J. R.; Mostafa, S.; Liu, J.; Sohn, Y.-h.; Roldan Cuenya, B. *Catal. Lett.* **2007**, *118*, 1.
(32) Kästle, G.; Boyen, H.-G.; Weigl, F.; Lengl, G.; Herzog, T.; Ziemann, P.; Riethmüller, S.; Mayer, O.; Hartmann, C.; Spatz, J. P.;

Möller, M.; Ozawa, M.; Banhart, F.; Garnier, M. G.; Oelhafen, P. *Adv. Funct. Mater.* **2003**, *13*, 853.
(33) Roldan Cuenya, B.; Baeck, S.-H.; Jaramillo, T. F.; McFarland, E. W. *J. Am. Chem. Soc.* **2003**, *125*, 12928.
(34) Damyanova, S.; Bueno, J. M. C. *Appl. Catal., A* **2003**, *253*, 135.
(35) Roldan Cuenya, B.; Croy, J. R.; Mostafa, S.; Behafarid, F.; Li, L.; Zhang, Z.; Yang, J. C.; Wang, Q.; Frenkel, A. I. *J. Am. Chem. Soc.* **2010**, *132*, 8747.
(36) Mansour, A. N.; Sayers, D. E.; Cook, J. W.; Short, D. R.; Shannon, R. D.; Katzer, J. R. *J. Phys. Chem.* **1984**, *88*, 1778.
(37) Friebel, D.; Miller, D. J.; O'Grady, C. P.; Anniyev, T.; Bargar, J.; Bergmann, U.; Ogasawara, H.; Wikfeldt, K. T.; Pettersson, L. G. M.; Nilsson, A. *Phys. Chem. Chem. Phys.* **2011**, *13*, 262.
(38) Merte, L. R.; Behafarid, F.; Miller, D. J.; Friebel, D.; Cho, S.; Mbuga, F.; Sokaras, D.; Alonso-Mori, R.; Weng, T.-C.; Nordlund, D.; Nilsson, A.; Roldan Cuenya, B. *ACS Catal.* **2012**, *2*, 2371.
(39) Behafarid, F.; Ono, L. K.; Mostafa, S.; Croy, J. R.; Shafai, G.; Hong, S.; Rahman, T. S.; Bare, S.; Roldan Cuenya, B. *Phys. Chem. Chem. Phys.* **2012**, *14*, 11766.
(40) Lei, Y.; Jelic, J.; Nitsche, L. C.; Meyer, R.; Miller, J. *Top. Catal.* **2011**, *54*, 334.
(41) Frenkel, A. I.; Yevick, A.; Cooper, C.; Vasic, R. *Annu. Rev. Anal. Chem.* **2011**, *4*, 23.
(42) Jentys, A. *Phys. Chem. Chem. Phys.* **1999**, *1*, 4059.
(43) Koningsberger, D. C.; Gates, B. C. *Catal. Lett.* **1992**, *14*, 271.
(44) Paredis, K.; Ono, L. K.; Behafarid, F.; Zhang, Z.; Yang, J. C.; Frenkel, A. I.; Roldan Cuenya, B. *J. Am. Chem. Soc.* **2011**, *133*, 13455.
(45) Vaarkamp, M.; Miller, J. T.; Modica, F. S.; Koningsberger, D. C. *J. Catal.* **1996**, *163*, 294.
(46) Zhang, Y.; Toebes, M. L.; van der Eerden, A.; O'Grady, W. E.; de Jong, K. P.; Koningsberger, D. C. *J. Phys. Chem. B* **2004**, *108*, 18509.
(47) Mager-Maury, C.; Bonnard, G.; Chizallet, C.; Sautet, P.; Raybaud, P. *ChemCatChem* **2012**, *3*, 200.
(48) McCabe, R. W.; McCready, D. F. *J. Phys. Chem.* **1986**, *90*, 1428.
(49) Safonova, O. V.; Tromp, M.; van Bokhoven, J. A.; de Groot, F. M. F.; Evans, J.; Glatzel, P. *J. Phys. Chem. B* **2006**, *110*, 16162.
(50) Chantaravitoon, P.; Chavadej, S.; Schwank, J. *Chem. Eng. J* **2004**, *97*, 161.
(51) McCabe, R. W.; Mitchell, P. J. *Appl. Catal.* **1986**, *27*, 83.
(52) Gentry, J.; Jones, A.; Walsh, T.; Sheffield, S. *J. Chem. Soc., Faraday Trans. I* **1980**, *76*, 2084.
(53) Lichtenberger, J.; Lee, D.; Iglesia, E. *Phys. Chem. Chem. Phys.* **2007**, *9*, 4902.
(54) Brewer, T. F.; Abraham, M. A.; Silver, R. G. *Ind. Eng. Chem. Res.* **1994**, *33*, 526.
(55) Chou, P.; Vannice, M. A. *J. Catal.* **1987**, *105*, 342.
(56) Xu, Y.; Shelton, W. A.; Schneider, W. F. *J. Phys. Chem. B* **2006**, *110*, 16591.
(57) Xu, Y.; Shelton, W. A.; Schneider, W. F. *J. Phys. Chem. A* **2006**, *110*, 5839.
(58) Ono, L. K.; Croy, J. R.; Heinrich, H.; Roldan Cuenya, B. *J. Phys. Chem. C* **2011**, *115*, 16856.
(59) Mars, P.; van Krevelen, D. W. *Chem. Eng. Sci.* **1954**, *3*, 41.
(60) Hendriksen, B. L. M.; Ackermann, M. D.; van Rijn, R.; Stoltz, D.; Popa, I.; Balmes, O.; Resta, A.; Wermeille, D.; Felici, R.; Ferrer, S.; Frenken, J. W. M. *Nat. Chem.* **2010**, *2*, 730.
(61) Endo, M.; Matsumoto, T.; Kubota, J.; Domen, K.; Hirose, C. *Surf. Sci.* **1999**, *441*, L931.
(62) Gong, X.-Q.; Liu, Z.-P.; Raval, R.; Hu, P. *J. Am. Chem. Soc.* **2004**, *126*, 8.
(63) Reuter, K.; Frenkel, D.; Scheffler, M. *Phys. Rev. Lett.* **2004**, *93*, 249701.
(64) Lashina, E. A.; Slavinskaya, E. M.; Chumakova, N. A.; Stonkus, O. A.; Gulyaev, R. V.; Stadnichenko, A. I.; Chumakov, G. A.; Boronin, A. I.; Demidenko, G. V. *Chem. Eng. Sci.* **2012**, *83*, 149.
(65) Jensen, R.; Andersen, T.; Nierhoff, A.; Pedersen, T.; Hansen, O.; Dahl, S.; Chorkendorff, I. *Phys. Chem. Chem. Phys.* **2013**, *15*, 2698.
(66) Schwartz, W. R.; Pfefferle, L. D. *J. Phys. Chem. C* **2012**, *116*, 8571.
(67) Müller, C. A.; Maciejewski, M.; Koeppel, R. A.; Tschan, R.; Baiker, A. *J. Phys. Chem.* **1996**, *100*, 20006.
(68) Seriani, N.; Pompe, W.; Ciacchi, L. C. *J. Phys. Chem. B* **2006**, *110*, 14860.
(69) Li, N.-H.; Sun, S.-G.; Chen, S.-P. *J. Electroanal. Chem.* **1997**, *430*, 57.
(70) Hellman, A.; Resta, A.; Martin, N. M.; Gustafson, J.; Trinchero, A.; Carlsson, P. A.; Balmes, O.; Felici, R.; van Rijn, R.; Frenken, J. W. M.; Andersen, J. N.; Lundgren, E.; Grönbeck, H. *J. Phys. Chem. Lett.* **2012**, *3*, 678.